


Characterizations on Precipitations in the Cu-Rich Corner of Cu-Ni-Al Ternary Phase Diagram

Yongxin Zhou¹, Chenyang Zheng¹, Jiankun Chen¹, Amin Chen¹, Lei Jia^{1,*} , Hui Xie² and Zhenlin Lu¹¹ School of Materials Science and Engineering, Xi'an University of Technology, Xi'an 710048, China² School of Materials Engineering, Xi'an Aeronautical University, Xi'an 710077, China

* Correspondence: xautjialei@hotmail.com

Abstract: Three kinds of Cu-Ni-Al alloys, whose chemical compositions are located in the Cu-rich corner of the isothermal section of the Cu-Ni-Al ternary phase diagram, were prepared by melting and casting firstly, and then solution and aging treatments were carried out. The microstructure was characterized and the competitive formation process of Ni-Al intermetallics were discussed. The results show that there are little amounts of NiAl phase at the grain boundary and needle- or particle-like Ni₃Al phase inside the Cu matrix in all the as-cast alloys, although they are in the single-phase area. Solution and aging treatments mainly result in the disappearance and precipitation of Ni₃Al phase, but the precipitations during aging are much smaller than those in the as-cast alloys. Thermodynamics and kinetics calculation indicate that the NiAl intermetallic wins out in the solidification process because of its lower change in Gibbs free energy, while Ni₃Al phase is first to precipitate during aging due to its lower formation enthalpy and required Al concentration. The most important contribution of this work is that it proves that intermetallics can precipitate from the so-called single-phase zone in the Cu-rich corner of the Cu-Ni-Al phase diagram, which is the necessary prerequisite for the realization of high strength and high electrical conductivity.

Keywords: Cu-Ni-Al alloy; heat treatment; thermodynamic calculation; precipitated phase



Citation: Zhou, Y.; Zheng, C.; Chen, J.; Chen, A.; Jia, L.; Xie, H.; Lu, Z. Characterizations on Precipitations in the Cu-Rich Corner of Cu-Ni-Al Ternary Phase Diagram. *Crystals* **2023**, *13*, 274. <https://doi.org/10.3390/cryst13020274>

Academic Editor: Anna Knaislova

Received: 9 January 2023

Revised: 3 February 2023

Accepted: 3 February 2023

Published: 4 February 2023



Copyright: © 2023 by the authors. Licensee MDPI, Basel, Switzerland. This article is an open access article distributed under the terms and conditions of the Creative Commons Attribution (CC BY) license (<https://creativecommons.org/licenses/by/4.0/>).

1. Introduction

A lead frame is of great importance in the integrated circuit, as it supports the bridge between the chip and the external conductor, as shown in Figure 1. Under normal conditions, copper alloys are used for lead frameworks because of their high ductility, thermal conductivity and electrical conductivity [1–3]. However, with the development of IC toward high integration and miniaturization, the number of components is increasing, while the distance between components is decreasing. In order to meet this serious requirement, enhancing the strength of materials on the basis of ensuring their high electrical conductivity, has become a hot topic of research for Cu-based materials. Up to now, the developed Cu alloys with both high strength and high electrical conductivity have mainly included Cu-Fe-(P), Cu-Ni-Si and Cu-Cr-(Zr) alloys [4–6]. Among them, Cu-Ni-Si series alloys are considered to be the most promising candidate for the high-performance integrated circuit, and their excellent comprehensive properties are mainly due to the precipitation of supersaturated Ni and Si atoms as δ -Ni₂Si (orthogonal structure) in a Cu-rich solid solution [7,8]. After that, the high electrical conductivity of the Cu matrix can be recovered significantly, while the strength can also be improved by the precipitation strengthening effect. Currently, the Cu-Ni-Si series alloy can usually achieve a tensile strength of 500–800 MPa and electrical conductivity of 30~65% IACS [9–11], which are much lower than the comprehensive properties of high strength and moderate electrical conductivity alloys (800 MPa and 60% IACS) [12]. When trying to further improve its strength, the conductivity drops rapidly, which can be attributed to the severe damage of the residual solution Ni and Si atoms to the conductivity of the copper matrix, especially the Si atoms. Hence, this is an obstacle to further obtaining a Cu-Ni-Si system with higher strength and conductivity.

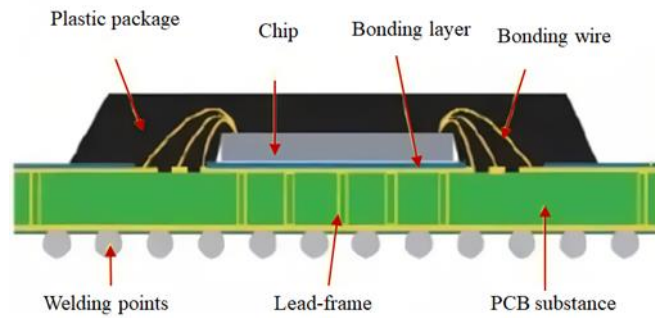


Figure 1. Schematic diagram of integrated circuit.

In order to deal with this matter, it is possible to select other solid solution elements that cause less damage to the conductivity of the copper matrix than Ni or Si, while they can also precipitate in the form of intermetallic compounds. According to this principle, the addition of Al element substituting for Si is expected to achieve a better more comprehensive performance. Firstly, when the same concentration of the residual solution atoms exists in the Cu matrix, the damage caused by Al to the electrical conductivity is much lower than that of Si element [13]. Secondly, Al has a relatively larger solubility than Si, and thus a higher Al alloying element can be used, which may produce more strengthening precipitations. Thirdly, there are also many stable intermetallic compounds in the Ni-Al system, such as Ni_3Al , NiAl_3 , NiAl and Ni_2Al_3 [14], which is similar to the Ni-Si system. Therefore, it is reasonable to believe that the Cu-Ni-Al system has much greater potential in terms of a higher strength and higher electrical conductivity than the Cu-Ni-Si system.

At present, it is regretful that no entire Cu-Ni-Al ternary phase diagram or similar research work has given any credible information about the precipitation behavior in the Cu-rich corner, which is the necessary prerequisite of Cu alloys with high strength and high electrical conductivity [15]. On the contrary, the isothermal section of the Cu-Ni-Al ternary system indicates that a single solution area exists in the Cu-rich corner at 500 °C, as shown in Figure 2 [16]. Therefore, if it can be confirmed that the Cu-Ni-Al ternary system can generate stable Ni-Al precipitates in the copper-rich area by heat treatments, it means that the potential of the Cu-Ni-Al system with high strength and high conductivity can finally be realized. However, there is very limited work on the Cu-Ni-Al system in this Cu-rich corner, and hence the present work just objectively studies the phase structure and precipitate behavior in this so-called single-phase zone.

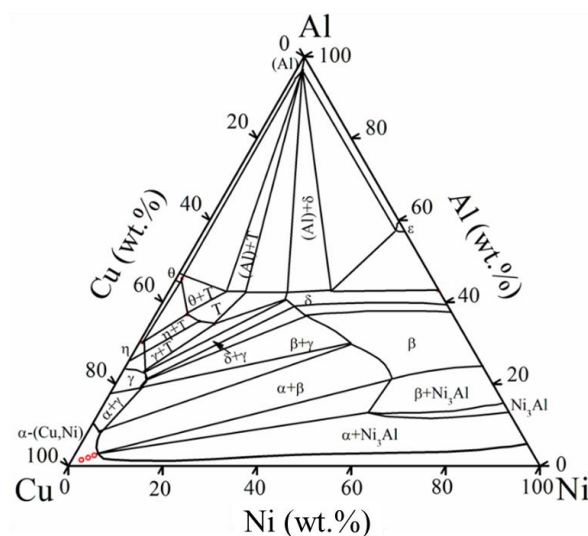


Figure 2. Isothermal section of Cu-Ni-Al ternary phase diagram at 500 °C [16].

2. Experimental Details

Three kinds of Cu-Ni-Al alloys with different chemical compositions, summarized in Table 1, were selected in the Cu-rich corner of the isothermal section of Cu-Ni-Al ternary system at 500 °C (Figure 2), where the mass ratio of Ni to Al was fixed at 1.5:1. Cu-Ni-Al alloys were prepared by the traditional smelting and casting method from Cu, Ni and Al substance blocks with purity higher than 99.99%. Before melting, all the raw materials were dried in a drying box at 50 °C, and the graphite crucible and mold were preheated at 200 °C for 2 h. The smelting process was carried out in AKPS-160/1 medium-frequency induction melting furnace, and firstly 15~20 mm thick charcoal powders were added to Cu blocks in the molten pool surface to inhibit oxidation. After Cu blocks melted, Ni and Al blocks were added and then held at about 1300 °C for 5 min to ensure that alloy melt was fully mixed with the aid of electromagnetic stirring. Before pouring, an appropriate amount of phosphor copper was added in the melts as a degassed agent, and the pouring temperature was about 1200 °C. Finally, the samples were cut into regular samples by wire cutting, and solid solution + aging treatments were carried out under the protection of Ar gas. According to the previous works on the heat treatments on Cu-Ni-Si alloys [5,17], the solution treatment was always performed at around 900 °C, while aging was carried out at 450–550 °C. In this work, heat treatments were carried out to investigate the phase transformation rather than regulate the properties of Cu-Ni-Al alloys, and hence the treating crafts were selected conservatively, which were 800 °C for 2 h and 500 °C for 4 h, respectively.

Table 1. Chemical composition and serial number of the Cu-Ni-Al alloys in this work.

Number	Nominal Composition	Content (wt.%)		
		Cu	Ni	Al
a	Cu-5.4Ni-3.6Al	91	5.4	3.6
b	Cu-4.2Ni-2.8Al	93	4.2	2.8
c	Cu-3.0Ni-2.0Al	95	3.0	2.0

Metallographic specimens were prepared by grinding, polishing and etching with the solution of 20% H_2O_2 (3%)-40% NH_3 (28%)-40% H_2O , and then observed by scanning electron microscopy equipped with energy-dispersive spectroscopy (SEM + EDS, Merlin Compact, Zeiss). Phase composition was analyzed by using X-ray diffractometer (XRD-7000, Shimadzu) at the two-theta range from 20 to 80°, and Cu target was used. Specific microstructure observation was conducted on transmission electron microscopy (HRTEM, JEM3010), and the samples were prepared by double spray thinning together with ion milling.

3. Results and Discussion

3.1. Microstructure and Phase Composition of As-Cast Alloys

Figure 3 shows the metallographic and SEM photos of the as-cast alloys with different Cu contents. It was found that their morphologies are similar and they are composed of matrix grains, precipitates inside the matrix and secondary phase on the grain boundaries. However, the variation in Cu content is slightly different. With the increase in Cu content, viz. the decrease in Ni and Al content, the amount of the precipitates inside the matrix grains decreases significantly, and their morphology also changes from needle-like to particle-like. At the same time, the second phase on the grain boundaries also changes in both amount and morphology, viz. changing from continuous netted-like to discontinuous particle-like morphology, as seen in Figure 3a–c. EDS analysis was carried out on both the particle-like phase inside and on the grain boundaries of the matrix grains, as shown in Table 2. It was found that the chemical composition and Ni/Al ratios are almost similar and close to 1:1, indicating that they may be the same phase. Because of the infinite solution characteristic between Cu and Ni, Cu is unable to solute in Ni-Al compounds. At the same time, the size of the secondary phase is too small to make sure the EDS spot fully focuses on

it, and the Cu element is detected in the secondary phase. However, XRD patterns of these alloys are basically consistent, and only the α -Cu (PDF:04-0836) phase can be detected, which may be mainly attributed to the limited amount of the precipitates and second grain boundary phase.

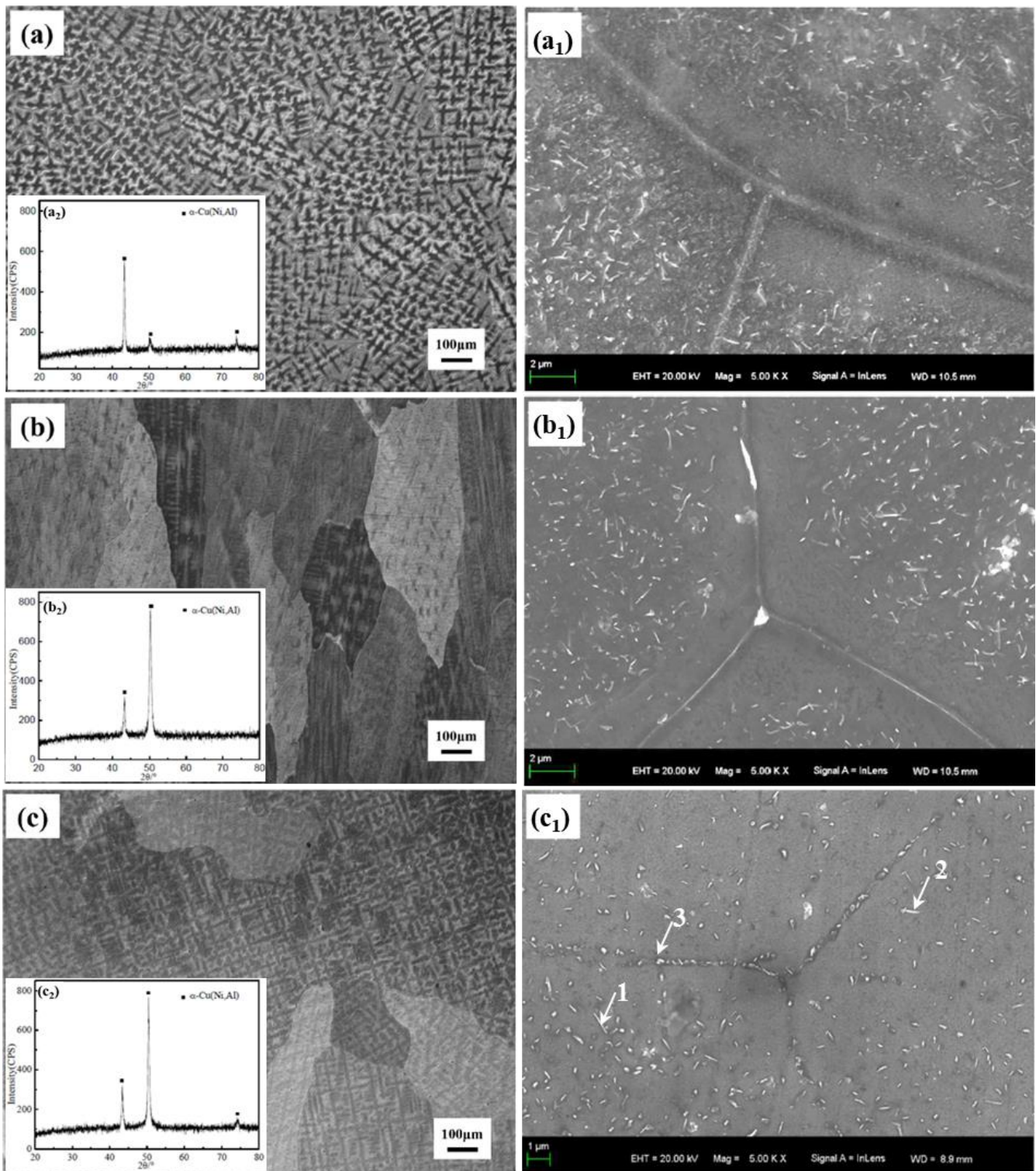
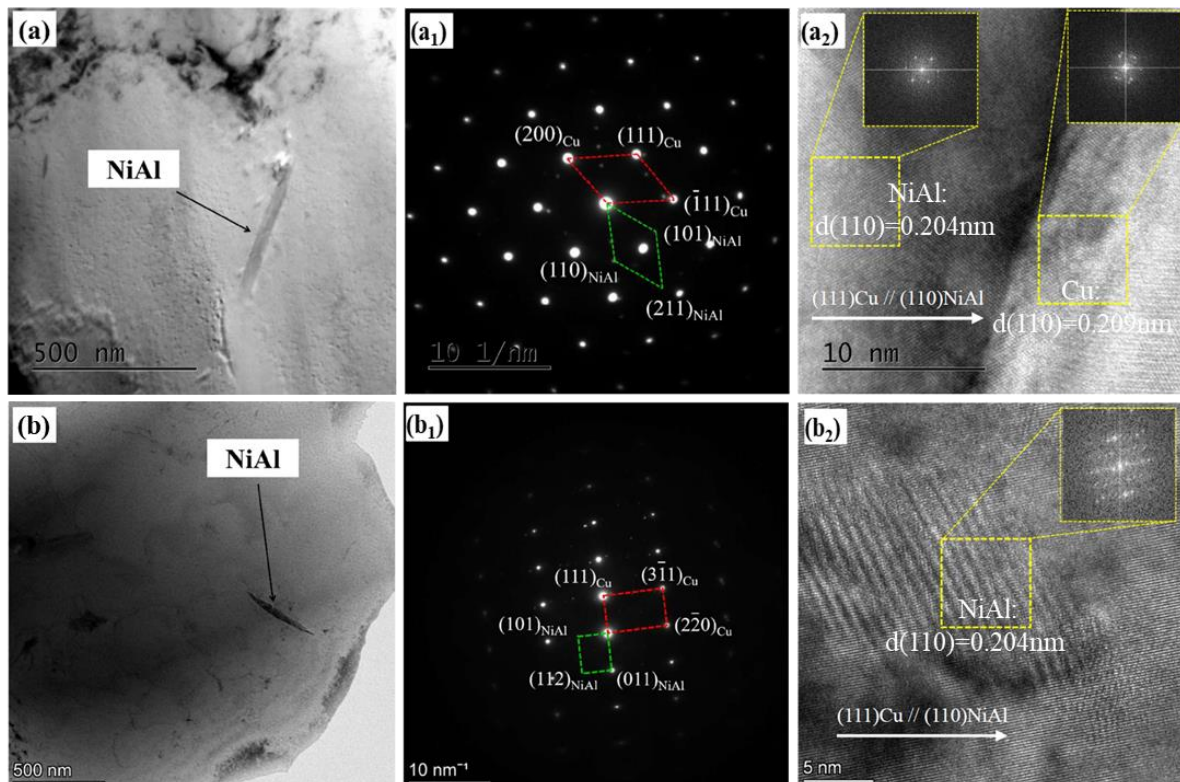


Figure 3. Microstructure of as-cast Cu-Ni-Al alloys with (a) 91%, (b) 93% and (c) 95% Cu content, respectively. The subscript (1) means the SEM image with high magnification.

Table 2. Results of EDS analysis on Cu-Ni-Al alloys with 95% Cu content, as shown in Figure 3c.

Points	Chemical Composition (at. %)			Atomic Ratio of Ni/Al
	Cu	Ni	Al	
1	84.90	7.28	7.82	0.931
2	84.78	7.35	7.87	0.934
3	84.17	7.15	8.69	0.823

To better understand the phase composition of the needle- and particle-like phases in the as-cast Cu-Ni-Al alloys with different Cu contents, TEM observation and selected area electron diffraction (SAED) analysis were carried out on the alloys with 91 wt% and 93% Cu, and the results are shown in Figure 4. It can be seen from the bright field image that a needle-like phase with a length of several hundred micrometers can be clearly seen in both of the two alloys (Figure 4a,b), and the SAED results indicate that both correspond to the NiAl phase with a B2 structure and the cell parameters are: $a = b = c = 0.289 \text{ nm}$, $\alpha = \beta = \gamma = 90^\circ$, as seen in Figure 4a₁,b₁. According to the Bramfitt's two-dimensional mismatch degree theory, when the mismatch degree is lower than 0.05, the orientation relationship between the secondary phase and matrix can be judged as a coherent interface; when that is between 0.05 and 0.25, the relationship is semi-coherent [18]. From the high-resolution images (Figure 4a₂,b₂), the mismatch value between the Cu matrix and NiAl phase can be calculated as 0.02, which is lower than 0.05, indicating there is a coherent relationship between them. These results also agree with the chemical composition confirmed by EDS in Table 2, approximately.

**Figure 4.** Transmission characterization of primary phase in as-cast (a) Cu-5.4Ni-3.6Al and (b) Cu-4.2Ni-2.8Al alloys, while the subscript 1 and 2 means the SAED patterns and HRTEM images.

3.2. Microstructure and Phase Composition of Heat-Treated Alloys

Figure 5 shows the results of microstructure characterization on Cu-4.2Ni-2.8Al alloys after solution and solution + aging treatments. Compared with the as-cast alloys (Figure 3b),

both the secondary phase on the grain boundaries and the precipitations inside the matrix have almost disappeared after solution treatment, as shown in Figure 5a. After aging treatment, there are a large amount of small white particles precipitated from both the grain boundaries and inside the matrix, as shown in Figure 5b. Further investigation by TEM observation and selective area electron diffraction shows that there are several NiAl phases with hundreds of nanometers and a needle-like shape, along with a large amount of Ni₃Al phases (face-centered cubic structure, $a = b = c = 0.378 \text{ nm}$, $\alpha = \beta = \gamma = 90^\circ$) with dozens of nanometers and a particle-like shape. The morphology and sizes of the NiAl phase are similar to those in the as-cast alloy, but Ni₃Al phase precipitates an as-new phase after solution and aging treatments. The mismatch value between the Cu matrix and Ni₃Al phase can be calculated from the high-resolution images (Figure 5c) as 0.12, which is between 0.05~0.25, indicating there is a semi-coherent relationship between them [18]. It is obvious that semi-coherent Ni₃Al intermetallics can successfully precipitate from the Cu-Ni-Al alloys by the aging treatment, demonstrating that this alloying system also has big potential for the combination of high strength and high electrical conductivity as with other precipitation-strengthening alloys. However, there is still a long way to go in the study of the regulation of the precipitating behavior of Ni-Al intermetallics until excellent comprehensive properties can finally be obtained.

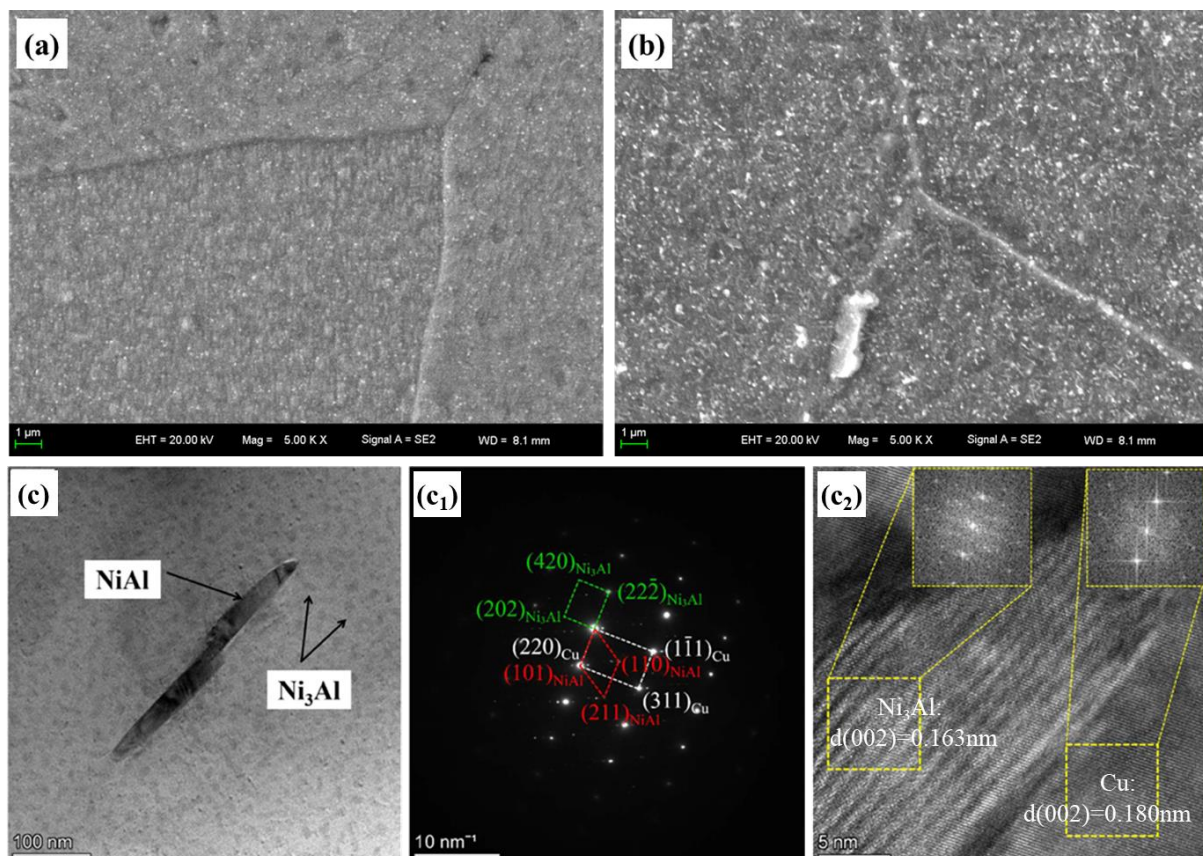


Figure 5. SEM images of (a) solid solution and (b) solid solution + aging Cu-4.2Ni-2.8Al alloy, and (c) specific TEM characterizations on the solid solution + aging state alloy, where (c₁) is SAED patterns and (c₂) is HRTEM image.

3.3. Thermodynamic Analysis on the Formation of Ni-Al Intermetallics

Although the entire ternary phase diagram of the Cu-Ni-Al system is not obtained, the formation sequence of Ni-Al intermetallics in the Cu-Ni-Al alloying melt during the cooling process can be approximately deduced from the as-cast and heat-treated microstructure

along with our previous work on the similar Cu-Ni-Si system [12,19], viz. NiAl phase is the product of solidification, while Ni₃Al phase precipitates from the aging treatment.

3.3.1. Solidification Process

During the cooling and solidification, the competitions between the Ni-Al intermetallics are always judged by the Gibbs free energy criterion. According to the Ni-Al phase diagram [14], the possible competitive reactions are shown as follows.



For a given chemical reaction, the change in Gibbs free energy at a specific temperature ($\Delta G, T$) can be calculated by the following Equation (5) [15]:

$$\Delta G, T = \sum v_i (G_i^\theta, T) \quad (5)$$

where v_i is the stoichiometric coefficient of the component i , which is negative for the reactants and positive for the products, while G_i^θ, T is the standard Gibbs free energy of component i at temperature T . For a substance at a specific temperature T , its standard Gibbs free energy can be expressed by the following equations [15]:

$$G_i^\theta, T = H_i^\theta, T - T \times S_i^\theta, T \quad (6)$$

$$H_i^\theta, T = \Delta_f H_i^\theta, 298 + \int_{298}^T c_{p,i} dT \quad (7)$$

$$S_i^\theta, T = S_i^\theta, 298 + \int_{298}^T c_{p,i} d \ln T + \sum \frac{L_{m,i}}{T_{m,i}} \quad (8)$$

where $\Delta_f H_i^\theta, 298$ and $S_i^\theta, 298$ are the standard molar formation enthalpy and entropy of component i at 298 K, respectively, and $c_{p,i}$ is the heat capacity at constant pressure, while $L_{m,i}$ and $T_{m,i}$ are the latent heat and temperature of the possible phase changes, respectively.

Since the melting point of Cu phase is around 1100 °C, the calculations on the change in Gibbs free energy using Equations (1)–(4) are only carried out in the temperature range of 1100 to 700 °C. By substituting all the thermophysical parameters (summarized in Table 3) from Reference [15] into the above equations, $\Delta G, T$ of the competitive reactions can be obtained, as shown in Figure 6a. It is obvious that the Gibbs free energy of reaction for the generation of NiAl is the lowest, suggesting that NiAl phase is the most likely phase during the solidification process of Cu-Ni-Al melts. This result is also in good agreement with the microstructure and phase composition of the as-cast alloys shown in Figures 3 and 4.

Table 3. Thermophysical parameters of Ni-Al intermetallics involved in this work [15].

Compounds	$\Delta_f H_i^\theta, 298$ (kJ/mol)	$S_i^\theta, 298$ (J/mol·K)	$C_{p,I}$ (J/mol·K)		
			a	b	c
Ni ₃ Al	−153.13	113.80	88.492	32.217	/
NiAl	−118.41	54.10	41.840	13.807	/
Ni ₂ Al ₃	−282.42	136.40	106.064	34.309	/
NiAl ₃	−150.62	110.67	84.098	35.146	/

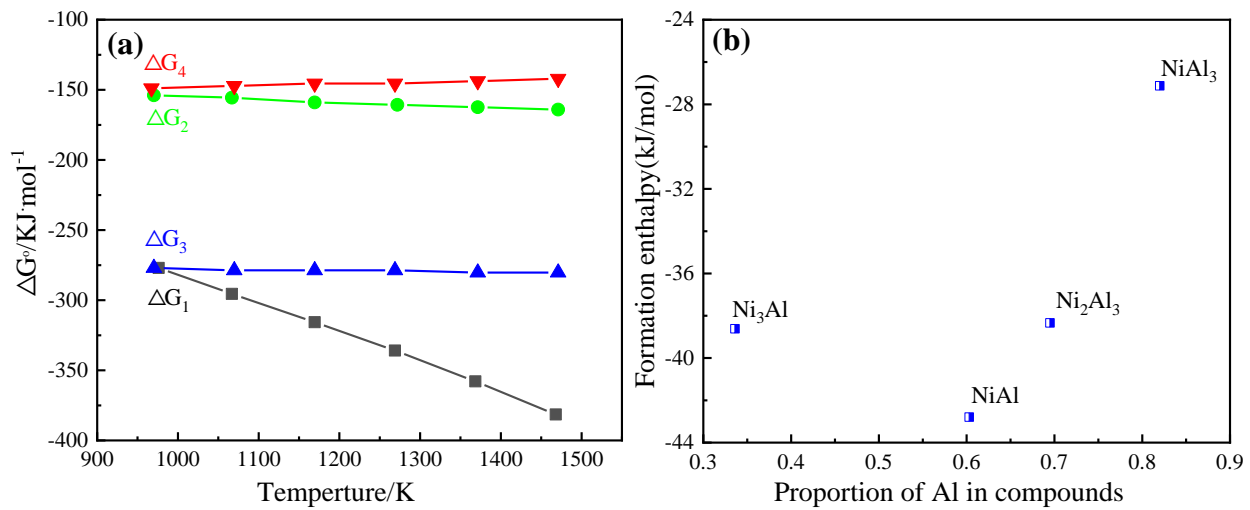


Figure 6. (a) Change in Gibbs free energy of potential reactions (1~4) at different temperatures and (b) formation enthalpy of different Ni-Al compounds.

3.3.2. Solid-State Process

For the solid-state phase transformation, especially when the intermetallics are precipitated from a supersaturated solution, the competitions among different phases need to be identified by the lowest formation enthalpies criterion. It can be seen from the Miedema model that the formation enthalpy of an intermetallic compound can be calculated by Equations (9) and (10) [20].

$$\Delta H_{ab} = \frac{f_{ab}\{x_a[1 + \mu_a x_b(\varphi_a - \varphi_b)]x_b[1 + \mu_b x_a(\varphi_b - \varphi_a)]\}}{\{x_a V_a^{2/3}[1 + \mu_a x_b(\varphi_a - \varphi_b)] + x_b V_b^{2/3}[1 + \mu_b x_a(\varphi_b - \varphi_a)]\}} \quad (9)$$

$$f_{ab} = \frac{2PV_a^{2/3}V_b^{2/3}\left\{\frac{q}{p}\left[\left(nws^{1/3}\right)_a - \left(nws^{1/3}\right)_b\right]^2 - (\varphi_a - \varphi_b)^2 - a\left(\frac{r}{p}\right)\right\}}{\left[\frac{1}{\left(nws^{1/3}\right)_a} + \frac{1}{\left(nws^{1/3}\right)_b}\right]} \quad (10)$$

where x_a and x_b are the volume fraction, V_a and V_b are the molar volumes, φ_a and φ_b are the electronegativity, and $\left(nws^{1/3}\right)_a$ and $\left(nws^{1/3}\right)_b$ are the Wigner–Seitz boundary electron concentrations of atoms A and B, respectively. Constants p , q , r , a and μ are determined by the chemical composition, electronegativity and electronic structure of the intermetallics. Substituting all the particular data from Reference [21], the formation enthalpy of the potential compounds in the Ni-Al system can be summarized in Figure 6b. It was found that the formation enthalpy of NiAl and Ni₃Al is much lower than that of other compounds, especially NiAl intermetallic, and hence the NiAl compound should be the most likely phase during the aging process. However, in the case of solid-state treatments, it is necessary to consider the difficulty of the diffusion of atoms in the solution matrix. It is regretful that the diffusion data of Ni and Al in Cu are absent, and hence the comparison between the diffusion ability can only be judged by using the atomic diameters and types of solid solution atoms. The Al atom is a substitutional solution in the Cu matrix [22], which is the same as Ni in Cu, but the atomic radius of Ni is smaller than that of Al, and thus it is reasonable to deduce that the diffusion ability of Ni is better than that of Al under the same temperature. In this case, Ni₃Al phase finally precipitates from the supersaturated Cu (Ni, Al) solution, since it has the lowest required Al concentrations and the second lowest formation enthalpy among all the potential Ni-Al intermetallics, as shown in Figure 5.

4. Conclusions

In this work, Cu-Ni-Al alloys with chemical composition located in the Cu-rich corner were prepared by the casting method and this was followed by heat treatments. Ni-Al intermetallic compounds were found and their phase composition was characterized firstly, and then the competitive formation behavior was discussed. The main conclusions are as follows:

1. Although the chemical composition is located in the single-phase area of the Cu-Ni-Al phase diagram, NiAl intermetallic phase can be formed at the grain boundary and the internal part of the Cu matrix, respectively. The higher the Ni and Al content is, the bigger the amount and size of the intermetallic compound.
2. Nano-sized Ni₃Al particles can precipitate from the solutioned Cu-Ni-Al alloys, indicating that the strength and electrical conductivity of Cu-Ni-Al alloys can be regulated by heat treatments, which is similar to other high-strength and high-conductivity Cu alloys.
3. NiAl phase is first to form in the solidification process since it has the minimum change in free Gibbs energy in all the potential competitive reactions of Ni-Al intermetallics, while Ni₃Al is more likely to precipitate from the supersaturated Cu (Ni, Al) matrix during the aging process because of the relative lower formation enthalpy and lower Al concentration required.

Author Contributions: Conceptualization, L.J. and H.X.; methodology, Y.Z. and L.J.; validation, Z.L. and H.X.; formal analysis, Y.Z. and L.J.; investigation, Y.Z., C.Z., A.C. and J.C.; resources, Y.Z.; data curation, C.Z., A.C. and J.C.; writing—original draft preparation, Y.Z. and C.Z.; writing—review and editing, L.J.; supervision, H.X. and Z.L.; project administration, Z.L.; funding acquisition, Y.Z. All authors have read and agreed to the published version of the manuscript.

Funding: This research and the APC were funded by Natural Science Foundation of China (51875453).

Institutional Review Board Statement: Not applicable.

Informed Consent Statement: Not applicable.

Data Availability Statement: Data will be available when required.

Acknowledgments: The authors are grateful to the National Natural Science Foundation of China (51875453) for their financial support.

Conflicts of Interest: The authors declare that they have no known competing financial interests or personal relationships that could have appeared to influence the work reported in this paper.

References

1. Chao, S.C.; Huang, W.C.; Liu, J.H.; Song, J.M.; Shen, P.Y.; Huang, C.L.; Hung, L.T.; Chang, C.H. Oxidation Characteristics of Commercial Copper-Based Lead Frame Surface and the Bonding with Epoxy Molding Compounds. *Microelectron. Reliab.* **2019**, *99*, 161–167. [\[CrossRef\]](#)
2. Xiao, X.; Huang, J.; Chen, J.; Xu, H.; Li, Z.; Zhang, J. Aging Behavior and Precipitation Analysis of Cu-Ni-Co-Si Alloy. *Crystals* **2018**, *8*, 435. [\[CrossRef\]](#)
3. Zhao, Z.; Xiao, Z.; Li, Z.; Qiu, W.; Jiang, H.; Lei, Q.; Liu, Z.; Jiang, Y.; Zhang, S. Microstructure and Properties of a Cu-Ni-Si-Co-Cr Alloy with High Strength and High Conductivity. *Mater. Sci. Eng. A* **2019**, *759*, 396–403. [\[CrossRef\]](#)
4. Wang, M.; Zhang, R.; Xiao, Z.; Gong, S.; Jiang, Y.; Li, Z. Microstructure and Properties of Cu-10 Wt% Fe Alloy Produced by Double Melt Mixed Casting and Multi-Stage Thermomechanical Treatment. *J. Alloys Compd.* **2020**, *820*, 153323. [\[CrossRef\]](#)
5. Suzuki, S.; Shibutani, N.; Mimura, K.; Isshiki, M.; Waseda, Y. Improvement in Strength and Electrical Conductivity of Cu-Ni-Si Alloys by Aging and Cold Rolling. *J. Alloys Compd.* **2006**, *417*, 116–120. [\[CrossRef\]](#)
6. Zhou, Y.; Yin, S.; Zhou, Q.; Chen, Z.; Xue, L.; Li, H.; Yan, Y. Improving High Temperature Properties of Cu-Cr-Y Alloy by Residual Cr Particles and Nano-Y₂O₃ Dispersions. *J. Mater. Res. Technol.* **2022**, *21*, 2976–2988. [\[CrossRef\]](#)
7. Chalon, J.; Guérin, J.D.; Dubar, L.; Dubois, A.; Puchi-Cabrera, E.S. Characterization of the Hot-Working Behavior of a Cu-Ni-Si Alloy. *Mater. Sci. Eng. A* **2016**, *667*, 77–86. [\[CrossRef\]](#)
8. Ma, M.; Li, Z.; Xiao, Z.; Jia, Y.; Meng, X.; Jiang, Y.; Hu, Y. Microstructure and Properties of Cu-Ni-Co-Si-Cr-Mg Alloys with Different Si Contents after Multi-Step Thermo-Mechanical Treatment. *Mater. Sci. Eng. A* **2022**, *850*, 143532. [\[CrossRef\]](#)

9. Liao, W.N.; Zhang, C.; Qiang, H.; Song, W.; Hu, Y. The Comprehensive Performance and Strengthening Mechanism of the Columnar Crystal Cu-Ni-Si Alloy after Two Large Deformation Rates of Cryogenic Rolling-Aging. *SSRN Electron. J.* **2023**, *936*, 168281. [[CrossRef](#)]
10. Monzen, R.; Watanabe, C. Microstructure and Mechanical Properties of Cu-Ni-Si Alloys. *Mater. Sci. Eng. A* **2008**, *483–484*, 117–119. [[CrossRef](#)]
11. Lei, Q.; Li, Z.; Wang, M.P.; Zhang, L.; Xiao, Z.; Jia, Y.L. The Evolution of Microstructure in Cu-8.0Ni-1.8Si-0.15Mg Alloy during Aging. *Mater. Sci. Eng. A* **2010**, *527*, 6728–6733. [[CrossRef](#)]
12. Xie, H.; Jia, L.; Lu, Z. Microstructure and Solidification Behavior of Cu-Ni-Si Alloys. *Mater. Charact.* **2009**, *60*, 114–118. [[CrossRef](#)]
13. Ghosh, G.; Miyake, J.; Fine, M.E. The systems-based design of high-strength, high-conductivity alloys. *JOM* **1997**, *49*, 56–60. [[CrossRef](#)]
14. Gale, W.F.; Totemeier, T.C. *Smithells Metals Reference Book*, 8th ed.; Butterworth-Heinemann: Oxford, UK, 2004; pp. 1703–1823.
15. Liang, Y.J.; Che, Y.C. *Handbook of Thermodynamic Data of Minerals*; Northeastern University Press: Shenyang, China, 1993. (In Chinese)
16. Baker, H. *ASM Handbook, Vol. 3, Alloy Phase Diagrams*; ASM International: Novelt, OH, USA, 1992; pp. 569–605.
17. Jia, L.; Lin, X.; Xie, H.; Lu, Z.L.; Wang, X. Abnormal improvement on electrical conductivity of Cu-Ni-Si alloys resulting from semi-solid isothermal treatment. *Mater. Lett.* **2012**, *77*, 107–109. [[CrossRef](#)]
18. Li, S.L.; Hu, P.; Liu, T.; Shi, Q.S.; Dang, X.M.; Hu, B.L.; Zhang, W.; Wang, K.S. Formation mechanism of coronal composite secondary phase in titanium-zirconium-molybdenum alloy. *Mater. Charact.* **2022**, *193*, 112235. [[CrossRef](#)]
19. Jia, L.; Xie, H.; Lu, Z.L.; Wang, X.; Lin, X. Experimental investigation on phase transformation of Cu-Ni-Si alloy melts during cooling. *Mater. Sci. Technol.* **2013**, *29*, 998–999. [[CrossRef](#)]
20. Miedema, A.R.; de Châtel, P.F.; de Boer, F.R. Cohesion in Alloys—Fundamentals of a Semi-Empirical Model. *Phys. B+C* **1980**, *100*, 1–28. [[CrossRef](#)]
21. Lei, Q.; Li, S.; Zhu, J.; Xiao, Z.; Zhang, F.; Li, Z. Microstructural Evolution, Phase Transition, and Physics Properties of a High Strength Cu-Ni-Si-Al Alloy. *Mater. Charact.* **2019**, *147*, 315–323. [[CrossRef](#)]
22. Haapalehto, M.; Pinomaa, T.; Wang, L.; Laukkanen, A. An atomistic simulation study of rapid solidification kinetics and crystaldefects in dilute Al-Cu alloys. *Comput. Mater. Sci.* **2022**, *209*, 111356. [[CrossRef](#)]

Disclaimer/Publisher’s Note: The statements, opinions and data contained in all publications are solely those of the individual author(s) and contributor(s) and not of MDPI and/or the editor(s). MDPI and/or the editor(s) disclaim responsibility for any injury to people or property resulting from any ideas, methods, instructions or products referred to in the content.